Available online at www.sciencedirect.com
SCIENCE DIRECT
Physics Letters A 353 (2006) 4–10
PHYSICS LETTERS A
www.elsevier.com/locate/pla

Coupling-induced cooperative behaviour in dynamic ferromagnetic cores in the presence of a noise floor

Adi R. Bulsara [a,*], John F. Lindner [d], Visarath In [a], Andy Kho [a], Salvatore Baglio [b], Vincenzo Sacco [b], Bruno Ando [b], Patrick Longhini [c], Antonio Palacios [c], Wouter-Jan Rappel [e]

[a] *Space and Naval Warfare Systems Center San Diego, Code 2363, 53560 Hull Street, San Diego, CA 92152-5001, USA*
[b] *Dipartimento di Ingegneria Elettrica Elettronica e dei Sistemi, Università degli Studi di Catania, Viale A. Doria 6, 95125 Catania, Italy*
[c] *Nonlinear Dynamics Group, Department of Mathematics, San Diego State University, San Diego, CA 92182, USA*
[d] *Physics Department, College of Wooster, Wooster, OH 44691, USA*
[e] *Physics Department, University of California at San Diego, La Jolla, CA 929093, USA*

Received 16 September 2005; received in revised form 22 November 2005; accepted 23 November 2005

Available online 19 December 2005

Communicated by C.R. Doering

Abstract

Recently, we have shown the emergence of oscillations in overdamped undriven nonlinear dynamic systems subject to carefully crafted coupling schemes and operating conditions. Here, we summarize experimental results obtained on a system of $N = 3$ coupled ferromagnetic cores, the underpinning of a "coupled-core fluxgate magnetometer" (CCFM); the oscillatory behaviour is triggered when the coupling constant exceeds a threshold value (bifurcation point), and the oscillation frequency exhibits a characteristic scaling behaviour with the "separation" of the coupling constant from its threshold value, as well as with an external target DC magnetic flux signal. The oscillations, which can be induced at frequencies ranging from a few Hz to high-kHz, afford a new detection scheme for weak target magnetic signals. We also present the first (numerical) results on the effects of a (Gaussian, exponentially correlated) noise floor on the spectral properties of the system response.

1. Introduction

Fluxgate magnetometers [1] have long afforded an inexpensive means of measuring magnetic fields in the 0.01 mT regime. Recently, laboratory prototype micro-fluxgates [4] with very good sensitivity have become available due to advances in the construction of very low noise "single-domain" ferromagnetic cores [2], as well as simplified time-domain readout schemes [3] that can be implemented with less complex readout and signal-conditioning electronics and lower on-board power requirements through the use of bias signals of significantly lower amplitude and frequency than traditional devices. In these readout scenarios, a known time-periodic bias signal having amplitude sufficient to sweep the ferromagnetic core between its saturation states, is applied to the device. A target DC signal then skews the underlying potential energy function; the ensuing asymmetry can be detected via traditional (second-harmonic) methods or the, recently described [3,4], residence times based readout strategy. In both techniques, a *supra*threshold bias signal, i.e. one having amplitude greater than the coercive field, and a frequency compatible with observation time, and internal flux-coupling constraints, are necessary. The sensitivity of the time domain based readout has been shown [4] to increase with lowered bias frequency and amplitude, within the above-mentioned constraints; these conditions are the opposite of the requirements for enhancing sensitivity in traditional (second harmonic) readouts, so that lower onboard power as well as simpler electronics can be implemented, with benefit, for the time domain readout case [4], subject, of course, to the practical constraints mentioned above.

We treat the single fluxgate magnetometer [3] as a nonlinear dynamic system by approximating the core as a single-domain obeying the evolution equation $\dot{x}[t] = -\nabla_x V[x]$, where $x[t]$ is

* Corresponding author.
E-mail address: bulsara@spawar.navy.mil (A.R. Bulsara).

0375-9601/$ – see front matter
doi:10.1016/j.physleta.2005.11.077

the (suitably normalized) macroscopic magnetization parameter, the overdot denotes time-derivative, and the potential energy function $V[x,t] = x^2[t]/2 - c^{-1}\ln[\cosh[c(x[t] + h[t])]]$. The temperature-dependent nonlinearity parameter c controls the topology of the potential function: the system becomes monostable, or paramagnetic, for $c < 1$, corresponding to an increase in the core temperature past the Curie point. The function $h[t]$ is an external target signal.

In two recent papers [5], we demonstrated that unidirectionally coupling overdamped bistable elements in a ring can lead to oscillatory behaviour when the coupling strength exceeds a critical value. In this work, we start by summarizing the experimental results on this topic, whose importance lies in the potential sensitivity enhancement when the system is "tuned" very close to the oscillation threshold (i.e. in the regime of very low frequency). Numerical studies of the system response in the presence of a noise-floor in each core, are also presented.

2. Coupled-core magnetometer: overview of deterministic behaviour

We start by writing down the dynamics for three unidirectionally (cyclically) coupled ferromagnetic cores, the underpinning of our so-called "coupled-core fluxgate magnetometer (CCFM)" ($i = 1,\ldots,3$, $x_4 \equiv x_1$):

$$\dot{x}_i = -x_i + \tanh\bigl[c(x_i + \lambda x_{i+1} + \varepsilon)\bigr], \tag{1}$$

where $x_i[t]$ represents the (suitably normalized) magnetic flux at the output (i.e. in the secondary coil) of unit i, and $\varepsilon \ll \Delta V$ is an externally applied DC "target" magnetic flux, ΔV being the energy barrier height (absent the coupling) for each of the elements (assumed identical for theoretical purposes). It is important to note [5] that the oscillatory behaviour occurs even for $\varepsilon = 0$, however when $\varepsilon \neq 0$, the oscillation characteristics change. These changes can be exploited for signal quantification purposes, the original motivation for our work. We reiterate that the oscillations do *not* occur for coupling $\lambda = 0$ due to the overdamped nature of the dynamics (1). The case of a time-periodic external magnetic flux signal has been discussed in a recent submission [6] and is not addressed in this Letter.

Under the above conditions, the system (1) displays oscillatory behaviour with the following features [5]: (1) The oscillations commence when the coupling coefficient exceeds a threshold value $\lambda_c = -\varepsilon - x_{\rm inf} + c^{-1}\tanh^{-1} x_{\rm inf}$, with $x_{\rm inf} = \sqrt{(c-1)/c}$; note that in our convention, $\lambda < 0$ so that oscillations occur for $|\lambda| > |\lambda_c|$. (2) The individual oscillations (in each elemental response) are separated in phase by $2\pi/N$ (we take $N = 3$ throughout this work, except where specifically stated otherwise), and have period $T_i = (1/\sqrt{\lambda_c - \lambda} + 1/\sqrt{\lambda_c - \lambda + 2\varepsilon})N\pi/\sqrt{cx_{\rm inf}}$, which shows a characteristic dependence on the inverse square root of the bifurcation "distance" $\lambda_c - \lambda$, as well as the target signal ε; these oscillations can be experimentally produced at frequencies ranging from a few Hz to high-kHz. (3) The *summed* output oscillates at period $T_+ = T_i/N$ and its amplitude (as well as that of each elemental oscillation) is *always supra*threshold, i.e. the emergent oscillations are strong enough to drive the core between its saturation states, *eliminating* the need to apply an additional bias signal for this purpose, as is done in single-core magnetometers. Increasing N changes the frequency of the individual elemental oscillations, but the frequency of the summed response is seen to be independent of N. (4) The residence times difference, i.e. the difference in the times spent by the system in its two stable magnetization states, can be computed as $\Delta t \approx (1/\sqrt{\lambda_c - \lambda} - 1/\sqrt{\lambda_c - \lambda + 2\varepsilon})\pi/\sqrt{cx_{\rm inf}}$, which vanishes (as expected) for $\varepsilon = 0$, and can be used as a quantifier of the target signal, analogous to the time-domain operation of the single fluxgate [3]. (5) The system responsivity, defined via the derivative $\partial\Delta t/\partial\varepsilon$, is found to increase dramatically as one approaches the critical point in the oscillatory regime; this suggests that careful tuning of the coupling parameter so that the oscillations have very low frequency, could offer significant benefits for the detection of very small target signals. Coupling, therefore, allows one to exploit the target-signal dependence of the emergent oscillations for detection and quantification purposes.

The oscillations observed from an experimental prototype [5,7] of a 3-core fluxgate magnetometer are quite striking (Fig. 1), and show good qualitative agreement with the results [5] of a simulation of the dynamics (1). Note that the amplitudes of the oscillations in the experiment are arbitrary compared to the model because the recorded voltages depend on the gains set in the coupling circuit. Of course, the magnetic flux in the model saturates between ± 1, but in real devices this quantity is not measured directly (a voltage readout is used).

In Fig. 2 we show the dependence of the oscillation frequency on the coupling strength; the characteristic (square root)

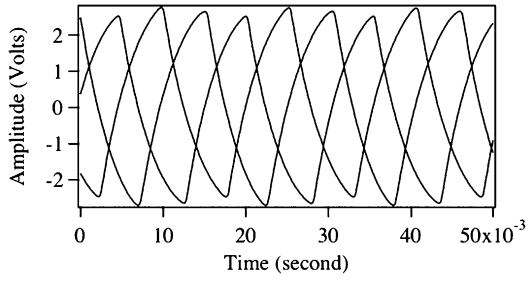

Fig. 1. Experimental response from 3 coupled PCB fluxgates. The curves correspond to each individual output $x_i[t]$. Note the $2\pi/3$ phase separation between the solutions, in conformance with the theory [5].

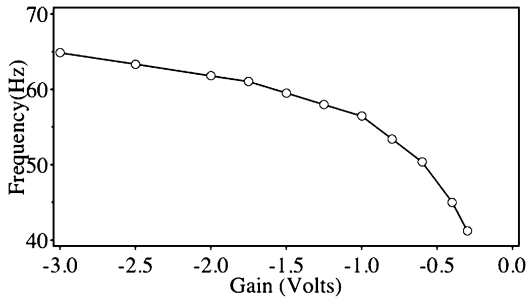

Fig. 2. Experimental result of frequency scaling of three coupled fluxgates with the applied field. The data agree quite well with the generalized 1/2-power model which corresponds to the calculated frequency $f_i = N/T_i$.

scaling is well-satisfied. As expected, decreasing the coupling strength increases the oscillation frequency. In practice, however, it is usually more convenient to use the residence times difference Δt as a quantifier of the target signal. The exact expressions (given above) show that, for a fixed coupling, Δt increases with increasing ε; essentially, the potential function is increasingly skewed so that the system spends a disproportionately large amount of time in one of its stable states. For small target signals, one may do a small-ε expansion to yield $\Delta t \approx (\lambda_{c0} - \lambda)^{-3/2}\pi\varepsilon/\sqrt{cx_{\inf}}$, where λ_{c0} now represents the critical coupling, absent the target signal. For a fixed ε, one observes, immediately, that the resolution (or responsivity $\partial\Delta t/\partial\varepsilon$) increases as one approaches the critical point (through adjusting the coupling parameter λ). This point is driven home in Fig. 3 wherein we show a family of responsivity curves as a function of the applied field for different coupling strengths; the vertical scale is the *ratio* of the upper residence time over the lower residence time. The responsivity curves could also be created by taking the residence times difference; we choose the ratio because it is dimensionless. The slopes of the curves indicate how responsive the coupled core system is to the applied field. As the coupling strength is increased toward the critical value, the responsivity curve becomes steeper. The greatest sensitivity is realized when the coupling strength is set closest to the critical value, but in this regime it can only detect a very small target field amplitude. Hence, the ability to tune the coupling to detect a range of target field strengths, must be a central feature of this mode of operation; when implemented, it presents a capability where one may tune the coupling to reduce the sensitivity and increase the operating range, or vice versa.

To summarize this section, it is clear that the coupled-core device yields its optimal performance in the very low frequency regime, close to the oscillation threshold; note that the experimental oscillations (Fig. 1) are at 65 Hz, far lower than the bias

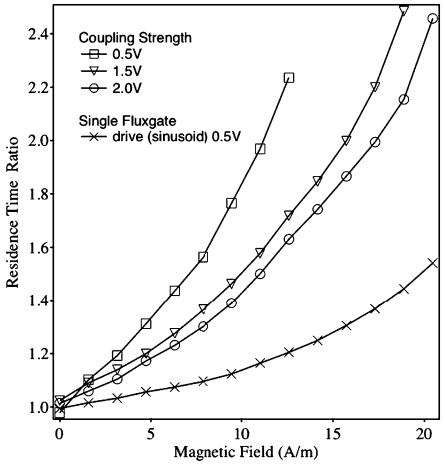

Fig. 3. Experimental responsivity curves, using the residence time ratio (RTR) vs. the applied target magnetic field ε for different coupling strengths. As expected, the coupled core system is less responsive as the coupling strength is increased (top 3 curves). The bottom curve is the responsivity of an "equivalent" single fluxgate magnetometer with bias signal amplitude selected to be slightly suprathreshold, thereby yielding the maximal sensitivity. Note that the RTR for the single fluxgate is, conveniently, frequency independent.

frequency that must usually be applied to conventional (single-core) fluxgates that are read out via the response power spectral density. The coupled system can be "tuned" to this regime by adjusting the coupling coefficient λ. This "tunability" of the optimal operating regime, if done carefully with consideration of the magnitude of target signals expected in a given application, is a big advantage (in addition to the absence of the bias signal) of the coupled system over its single element counterpart. Note that one may, in fact, perform an approximate conversion [4] of the resolution to a more conventional sensitivity (typically characterized via a noise floor). While this conversion has not yet been carried out for the 3-fluxgate system, we note that each individual fluxgate in our experiment had a laboratory noise-floor of 10–14 pT/$\sqrt{\text{Hz}}$ at 1 Hz, when read out via the residence times difference technique [4]. More details about the experimental setup and results will appear in a forthcoming publication [7].

3. The effects of a noise floor

In any practical application, one always has to contend with noise that arises from two sources: the (magnetic) noise floor of each sensor, and noise that contaminates the target signal. Here we will consider the effects, solely, of the noise floor, assuming it to be Gaussian band-limited noise having zero mean, correlation time τ, and variance σ^2. This type of noise is a good approximation (except for a small $1/f$ component at very low frequencies) to what is actually observed in the experimental setup. Theoretically, colored noise $F[t]$ appears as an additive term on the right-hand side of each of Eq. (1) and is characterized by [12] $\langle F[t]\rangle = 0$ and $\langle F[t]F[s]\rangle = (D/\tau) \times \exp[-|t-s|/\tau]$, where $D = \sigma^2\tau$ is the noise intensity, and the "white" limit is obtained for vanishing τ, although practically, the white noise is always band-limited. We assume (for simplicity) the same noise parameters for each core, however the noise is taken to be uncorrelated from core-to-core.

We start with a rapid recapitulation of some theoretical [3] and experimental [4] observations stemming from our work with single RTD fluxgates. The voltage signal from the fluxgate has been shown [4] to have a noise component that can be well-approximated by a Gaussian distribution. However, the individual residence times have noise components which are, in general, non-Gaussian; they have noise-dependent tails and, with increasing noise intensity the tails get longer. This is a feature that is quite common to two-state devices; in particular, the inverse Gaussian distributions that describe the dynamics of "integrate-fire" neurons have this structure. Our earlier experimental work [3] verified these features for a single-core fluxgate magnetometer read out using the residence times approach, and also showed that decreasing the noise intensity (alternatively, increasing the bias amplitude A) reduced the tail and made the distributions more Gaussian-like. Of course, this comes at the price of reduced sensitivity (since the sensitivity in this case is inversely proportional to the bias amplitude). A careful optimization of geometrical and other core parameters can also lower the noise in the voltage signal.

To better understand the ramifications of background noise, we have introduced [3] the (critical, to a practical system) observation time $T_{\rm ob}$, and defined a response signal-to-noise ratio (SNR) which is directly proportional to $\sqrt{T_{\rm ob}}$. A longer observation time leads to an enhanced response (to very weak target signals), however, practical constraints may limit $T_{\rm ob}$. One can increase the bias frequency ω (when dealing with only a single device), thereby increasing the number of crossing events and improving the statistics of the measurement process, however this implies a larger onboard power requirement. Hence, in a practical application, one must strike a balance between the physical constraints (e.g. onboard power, noise from the bias signal generator) and the need to carry out a reliable measurement of the mean RTD. The practical configuration is also, of course, heavily dependent on the amplitude (relative to the energy barrier height) of the target signal ε to be quantified.

3.1. Fixing the noise correlation time τ

As already mentioned, the simple case of (additive) white noise is realized, in theory, in the limit of vanishing correlation time τ, when the noise has an infinitely large bandwidth. Of course, in practice, either experimentally or computationally, this bandwidth is limited. In the presence of a small noise floor, one observes that the noise floor manifests itself in fluctuations of the "rest" states of each core, about the deterministic mean values $\pm b$ (these are the minima of the single core potential energy function) which can readily be calculated [3]. Numerical simulations of the coupled system show that the threshold crossings are quite sharp and unambiguous (as long as the noise is not too strong). This is a direct consequence of the very low time constant τ_F (usually $\ll \tau$) of each core; to all intents and purposes, each element behaves like a static nonlinearity, with near-instantaneous switching events.

We now present the first results from the numerical simulations of the coupled system (1) in the presence of additive, Gaussian, band-limited white noise. For convenience, the nonlinearity parameter c is also taken to be the same throughout. Further, we consider only the case of zero target signal (i.e. $\varepsilon = 0$) so that the system is a priori symmetric.

The power spectral density (PSD) of any of the solutions $x_i[t]$ shows interesting features, as seen in Fig. 4. Specifically, it appears to share much in common with what is observed in renewal processes [8]. Given the near-instantaneous transition between the upper and lower thresholds, preceded by a relatively slow transition to the threshold (this is readily observable in the deterministic time series [5]), and coupled with the (not-unreasonable) assumption of independent crossing events, the renewal description seems to be a good one. The features of the PSD are better explained with reference to Fig. 5 which shows the modal switching frequency (the location, f_M, of the fundamental peak in the corresponding PSD) of a *single* element in the $N = 3$ ring, as a function of the noise intensity for two values of the coupling coefficient bracketing its critical value. On this figure, we also plot (for comparison purposes) the characteristic (Kramers) noise-induced hopping rate, which is numerically computed for a single uncoupled element in the array. For the subthreshold case, the PSD for any choice of parameters shows a "knee" at the fundamental (noise-induced) oscillation frequency f_M; with increasing noise, the spectrum becomes flatter, approaching the limit where the maximum

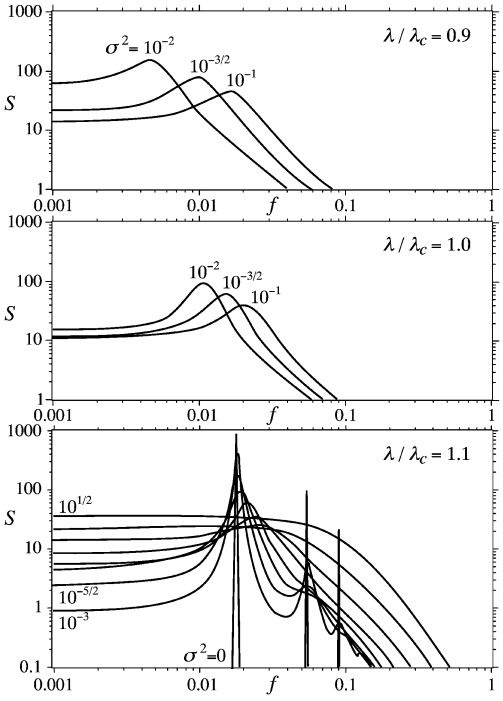

Fig. 4. Simulated power spectral densities (PSDs) for three values of coupling, for various values of noise. Curves are labeled by noise variances, which increase by factors of $\sqrt{10}$, while the noise correlation time $\tau = 1$, and the nonlinearity $c = 3$. Critical coupling $\lambda_c = -0.4345$, as computed in Section 1. Sharp peaks (bottom panel) correspond to the deterministic oscillation frequency and its (odd) higher harmonics.

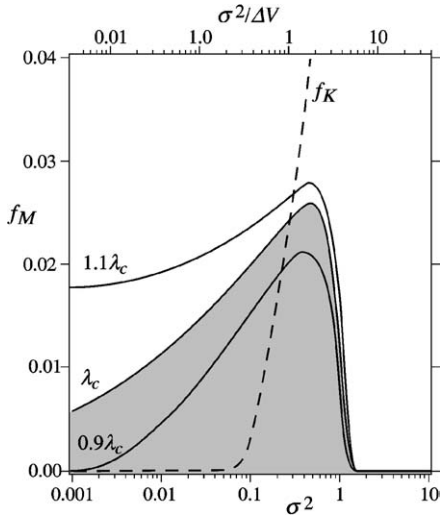

Fig. 5. Simulated modal oscillation (or switching) frequency f_M of a *single* fluxgate in the $N = 3$ configuration as a function of noise intensity σ^2 (normalized to potential barrier height ΔV of a single uncoupled fluxgate, on top scale). f_M denotes location of peak in the corresponding PSD (see e.g. Fig. 4). Dashed curve is the (numerically computed) Kramers rate f_K for a single *uncoupled* element. Grey area corresponds to the subcritical (nonoscillating, in the absence of noise) regime. Other parameters as Fig. 4.

spectral amplitude occurs at zero frequency for large noise. For the suprathreshold case we have, already, a deterministic oscillation frequency (shown as a spike, together with its 3rd and 5th harmonics in Fig. 4), and the effect of the noise is to replace this spike with a broad (and shifted) peak and its odd (because the system is symmetric) harmonics; note that the higher harmonics are not visible unless the noise is very small. For very small noise intensities, the modal oscillation frequency (i.e. the inverse mean of the period distribution function) does not deviate appreciably from the deterministic oscillation frequency; this is also evident in the top curve of Fig. 5 wherein one observes a finite oscillation frequency even for zero noise, as expected. With increasing noise intensity, however, the mean oscillation frequency becomes a function of the noise and separates itself from the deterministic frequency. Simultaneously (with increasing noise), the peak amplitude (in the PSD) decreases until, past the Kramers rate f_K, the PSD has its maximum amplitude at zero frequency (for any value of λ), as would be expected; this is clearly evident in the bottom panel of Fig. 4. The above features are the subject of ongoing investigations. The occurrence of hopping events in the subcritical regime, where the deterministic system is quiescent is, clearly, a case of purely noise-induced switching. In Fig. 6 we plot the relative spectral amplitude $\Delta S = (S[f_M] - S_0)/S_0$ of the frequency feature at f_M in the PSD as a function of noise; for the subthreshold case, this amplitude is taken at the "knee" of the PSD, and we define $S_0 \equiv S[f = 0]$. Note the coherence resonance (CR)-like feature (recall that there is no time-periodic target signal present) in the subthreshold case [9]; this behaviour is not seen in the suprathreshold case, quite analogous to observations on driven bistable systems. An important feature about the CR in the present case is worth pointing out. In conventional CR [9], a clear separation of time-scales between "fast" and "slow" variables permits one to separate the system in the low-frequency oscillation regime (close to the onset of the noisy bifurcation to CR). No such (formal) separation is possible in the current system with all the cores described by the system (1) having the same time constant τ_F (of course, one can fabricate devices having widely dissimilar time constants but this would complicate the dynamics and our analyses, as well as the design of actual systems based on our work). However, a glance at the theoretical (numerical) solutions of the system (1) immediately reveals that, close to the onset of the oscillations at least, the elements evolve almost one at a time, while the remaining elements remain approximately at rest (except for small intrawell jitter caused by the noise floor) in one of their stable steady states. As soon as the active element has switched states, it remains confined to that well (with some intrawell jitter), while the next one begins its switching. This is the mechanism of the soliton-like "ripple" that travels through the ring; however, it implies, also, that the dynamics introduces a de facto separation of time scales from element to element as manifested in this sequential switching behaviour. An analytic solution of the system in this case might be possible, for very small noise at least, but is complicated by the fact that, with increasing noise, the dynamical behaviour just described becomes more complex and the aforementioned sequential evolution is no longer so clear-cut. This is a problem that is, currently, under intense theoretical investigation.

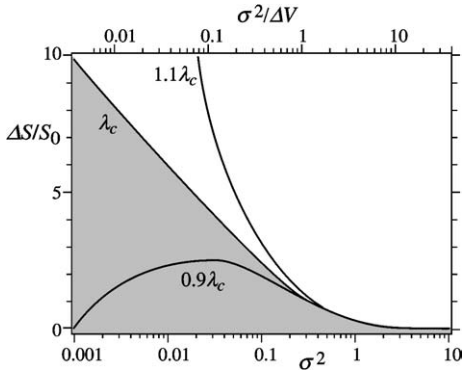

Fig. 6. Simulated spectral amplitude at frequency feature normalized to the spectral amplitude at zero frequency (see text), vs. noise intensity σ^2 (normalized by the energy barrier height on top scale), for same values of coupling λ as Fig. 5 $c = 3$, $\lambda_c = -0.4345$.

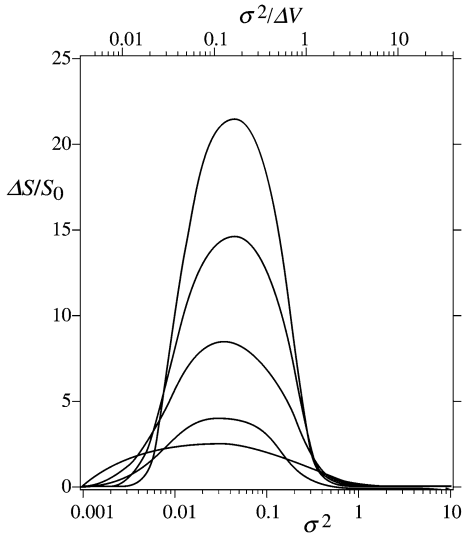

Fig. 7. Same as Fig. 6 but showing the simulated effects of increasing N; (bottom to top peaks) $N = 3, 5, 7, 9, 11$. $c = 3$, $\lambda = 0.9\lambda_c = -0.39105$, $\tau = 1$.

Finally, we address the issue of increasing the number of elements in the coupled array. We arrange the elements in a ring (a one-dimensional chain with periodic boundary conditions). As already mentioned (Section 1), changing N leads to a proportionate scaling of the individual frequencies of the component elements, however, the summed output oscillates at a frequency independent of N. Fig. 7 shows the normalized spectral amplitude at the fundamental frequency feature in the output PSD of a single element for 5 different N values, in the subthreshold regime. Clearly, analogously to the array enhanced SR effect [10], increasing N leads to an enhancement in the spectral response of *individual* elements in the array but *not* for the summed output. Fig. 8 provides an intuitive explanation for this behaviour. The time series panels indicate that the $N = 3$ time-series output displays (for the value of noise intensity considered in this plot) more incoherence in its switching dynamics than the $N = 9$ case, probably because in the larger ring, the "soliton" takes longer to propagate around the ring and

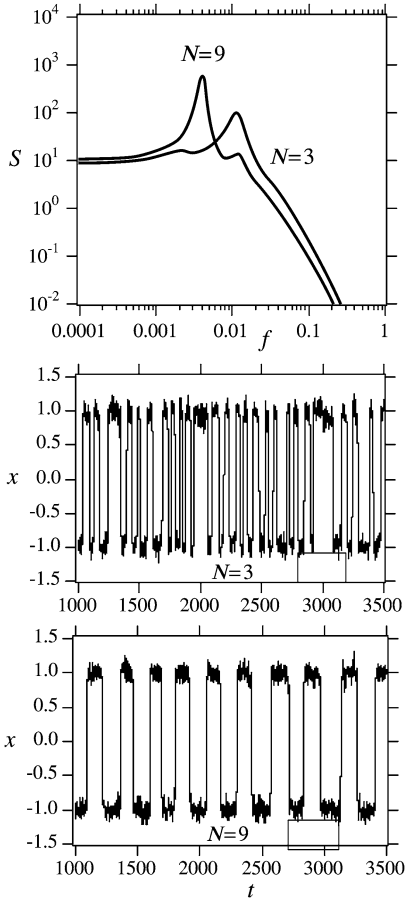

Fig. 8. Simulated response of a single element in the $N = 3$ and $N = 9$ coupled arrays. Lower panels show the temporal response and top panel shows the power spectral densities. Parameters correspond to those of Fig. 7 with the noise intensity parameter set to the value at which the curves of Fig. 7 are peaked.

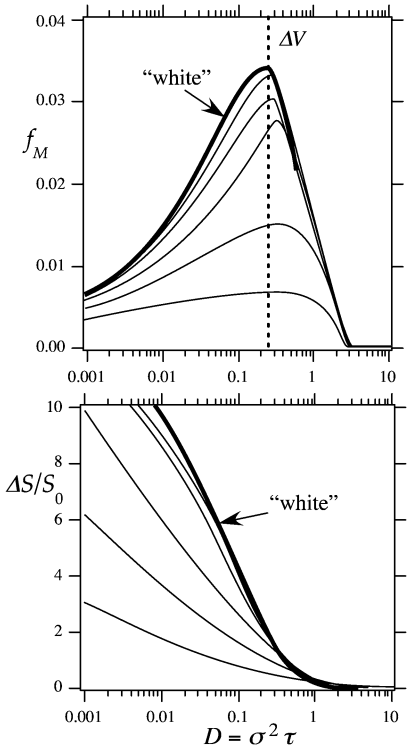

Fig. 9. Same as Figs. 5 and 6 but showing the simulated effects of increasing noise color, with noise correlation time decreasing logarithmically from bottom to top, $\tau = 10, \sqrt{10}, 1, 1/\sqrt{10}, 1/10$. Thick lines illustrate white noise limits. Vertical dashed line is the barrier height $\Delta V = 0.2698$. Coupling strength $\lambda = \lambda_c$.

is, thus, isolated "from itself". The more coherent (i.e. periodic, in this case) temporal response manifests itself in a higher peak at the fundamental response frequency in the power spectral density; the shift (as predicted by the deterministic theory of Section 2) in the location of this peak is also apparent, and is a direct result of the "soliton" taking longer to circumnavigate the ring with increasing N. These features, a probable manifestation of array enhanced coherence resonance [11] are, also, being investigated.

3.2. Varying the noise correlation time

The preceding treatment assumed that the external noise, while independent from site-to-site, had its correlation time fixed at $\tau = 1$. In practice, the individual device time constants τ_F are of considerable importance in determining the dynamical behaviour and, in fact, determine whether the system sees the noise as white or colored. The quantity τ_F^{-1} defines the "bandwidth" of each switching element. In well-made devices one typically has $\tau_F \approx 10^{-6}$ or even somewhat less, corresponding to a very sharp hysteresis loop and near instantaneous switching between stable steady states. The noise, however, is almost always band-limited with typical sources being materials noise and noise in the readout electronics (we do not consider, here, the case of noise contaminating an externally applied target signal). Typically, the noise bandwidth τ^{-1} is smaller than the bandwidth of each switching element. Hence, given a noise source (or even a deterministic external signal having frequency smaller than τ_F^{-1}) of sufficient strength to permit switching in a single system element (in this case, one of the cores), the system can be treated as a static nonlinearity with its switching dynamics predicated entirely on the noise bandwidth τ^{-1}. Then, for a single device, we are lead to a simple description in terms of the noise as a dynamic Ornstein–Uhlenbeck process controlled by the decay constant τ^{-1} and a Gaussian noise source with variance σ^2, the effect of the nonlinear device being simply to set the "switching threshold" that has to be crossed by the (linear) noise dynamics. This procedure is well-established and has been applied to a number of 1D systems [13]. For the coupled system (1), the situation is far more complex and an analytic technique for solving the noisy system and unlocking the CR behaviour referenced above does not, yet, exist. Here, however, we present some preliminary (numerical) results showing how the introduction of noise "color" changes the behaviour of some of the spectral properties described above. When carrying out numeric simulations, we are careful to keep the simulation step-size Δt much less than the correlation time τ. We typically choose $\Delta t = 0.004$.

Fig. 9 is analogous to Figs. 5 and 6 but shows the effects of changing the noise correlation time for the $N = 3$ ring at

its critical coupling $\lambda = \lambda_c$. In this figure, the noise correlation times decrease geometrically by factors of $\sqrt{10}$ from bottom curves to top curves. The thick lines are the $\tau \to 0$ "white" noise limits. The decrease in spectral amplitude (lower panel) is, of course, an already observed feature in single overdamped bistable systems subject to correlated noise and a time-sinusoidal driving signal [14].

4. Concluding remarks

This Letter describes a novel way to couple nonlinear dynamic devices (in this case, overdamped bistable elements) that cannot switch between their stable attractors unless driven. Unidirectional coupling, combined with a cyclic boundary condition and a choice of initial conditions such that at least one element has a different initial state from the rest, leads to sequential switching behaviour in the chain. The result is the propagation of a periodic disturbance, reminiscent of a soliton, through the chain. The behaviour is observed for even and odd N and shows some novelties when N becomes very large, as well as when the sign of the coupling coefficient is changed in a large N array [15]. We have observed this behaviour in our laboratory setup involving 3 coupled ferromagnetic cores, the underpinnings of a coupled-core fluxgate magnetometer that is being developed for the detection of weak target (DC and time-periodic) magnetic flux signals. The effects of an additive (and, in general, correlated) noise floor in each core are quantified here, for the first time. It is important to note that, in practice, the coupling circuits draw power, so that a truly "power-less" operation of a real coupled system would be impossible, as dictated by fundamental conservation laws. The effects described in this Letter (with our particular coupling topology) are, however, generic to a very wide class of nonlinear coupled systems whose individual dynamics are derivable via the gradient of a potential energy function $V[x]$ (bistable, for the case of this work). It is clear, also, that much theoretical work aimed at quantifying the noisy dynamics of such systems, remains; introducing additional complexities (e.g. dissipation, that would raise the dimensionality of each constituent element) is likely to yield a richness of behaviour that still remains undiscovered.

Acknowledgements

We gratefully acknowledge support from the Office of Naval Research (Code 331) as well as the ILIR program at SPAWAR Systems Center. A.R.B. acknowledges a fruitful interaction with B. Lindner (Dresden). J.F.L. thanks The College of Wooster for making possible his sabbatical at Georgia Tech.

References

[1] See, e.g.: W. Bornhofft, G. Trenkler, in: W. Gopel, J. Hesse, J. Zemel (Eds.), Sensors, A Comprehensive Survey, vol. 5, VCH, New York, 1989; P. Ripka, Magnetic Sensors and Magnetometers, Artech House, Boston, 2001, for good reviews.
[2] R. Koch, J. Deak, G. Grinstein, Appl. Phys. Lett. 75 (1999) 3862; R. Koch, J. Rozen, Appl. Phys. Lett. 78 (2001) 1897.
[3] A. Bulsara, C. Seberino, L. Gammaitoni, M. Karlsson, B. Lundqvist, J.W.C. Robinson, Phys. Rev. E 67 (2003) 016120.
[4] B. Ando, S. Baglio, A. Bulsara, V. Sacco, IEEE Trans. Instrum. Meas. 54 (2005) 1366; B. Ando, S. Baglio, A. Bulsara, V. Sacco, IEEE Sensors 5 (2005) 895; B. Ando, S. Baglio, A. Bulsara, V. Sacco, Measurement 38 (2005) 89.
[5] V. In, A. Bulsara, A. Palacios, P. Longhini, A. Kho, J. Neff, Phys. Rev. E 68 (2003) 045102(R); A. Bulsara, V. In, A. Kho, P. Longhini, A. Palacios, W.-J. Rappel, J. Acebron, S. Baglio, B. Ando, Phys. Rev. E 70 (2004) 036103.
[6] V. In, A. Bulsara, A. Palacios, P. Longhini, A. Kho, Phys. Rev. E (2005), submitted for publication.
[7] V. In, V. Sacco, A. Kho, S. Baglio, B. Ando, A. Bulsara, A. Palacios, IEEE Sensors (2005), in press.
[8] T. Lukes, Proc. Phys. Soc. London 78 (1961) 153; S. Lowen, M. Teich, Phys. Rev. E 47 (1993) 992.
[9] A. Pikovsky, J. Kurths, Phys. Rev. Lett. 78 (1997) 775; B. Lindner, L. Schimansky-Geier, Phys. Rev. E 60 (1999) 7270; B. Lindner, L. Schimansky-Geier, Phys. Rev. E 61 (2000) 6103.
[10] J. Lindner, B. Meadows, W. Ditto, M. Inchiosa, A. Bulsara, Phys. Rev. Lett. 75 (1995) 3; J. Lindner, B. Meadows, W. Ditto, M. Inchiosa, A. Bulsara, Phys. Rev. E 53 (1996) 2081.
[11] Y. Shinohara, T. Kanamaru, H. Suzuki, T. Horita, K. Aihara, Phys. Rev. E 65 (2002) 051906.
[12] See, e.g.: P. Hanggi, P. Jung, Adv. Chem. Phys. 89 (1995) 239.
[13] R. Bartussek, P. Jung, P. Hanggi, Phys. Rev. E 49 (1994) 3930; A. Bulsara, M. Inchiosa, L. Gammaitoni, Phys. Rev. Lett. 77 (1996) 2162.
[14] L. Gammaitoni, E. Menichaella-Saetta, S. Santucci, F. Marchesoni, C. Presilla, Phys. Rev. A 40 (1989) 2114.
[15] J. Lindner, A. Bulsara, Phys. Rev. Lett. (2005), submitted for publication.